Electronic Supplementary Material (ESI) for Environmental Science: Nano.

Electronic supporting information

Coating ligands mediated dynamic formation of natural organic matter (NOM) corona on engineered nanoparticles in environments

Chuan-Wang Yang, Li Yuan*, Xin Zhang, Hong-Zhi Zhou, Guo-Ping Sheng*

CAS Key Laboratory of Urban Pollutant Conversion, Department of Environmental
Science and Engineering, University of Science & Technology of China, Hefei
230026, China

*** Corresponding authors:**

Li Yuan
E-mail: ly2016@ustc.edu.cn

Guo-Ping Sheng
E-mail: gpsheng@ustc.edu.cn

This electronic supporting information contains 22-page document, including materials and methods, 14 figures, 2 tables, references, and this cover page.

Atomic force microscopy (AFM) characterization

AFM characterization of the pure and HA-coated AgNPs was carried out on an atomic force microscopy (SmartSPM-1000, AIST-NT) according to the previously reported method.[1, 2] Nanoparticles were firstly incubated with HA (125 mg-C/L) for 24 h and washed with ultrapure water twice to remove unbounded HA. For pure nanoparticles, three AgNPs were washed with ultrapure water one time. After centrifugation at 3000 g × 5 min, the concentrated nanoparticle suspensions were dropped onto freshly cleaved mica surface and dried in a vacuum for 30 min. The resonance frequency of AFM cantilever was tuned at 116 kHz using tapping mode.

Data processing for UV-vis and Raman spectra

To identify the peak position of UV-vis spectra of AgNPs, Gaussian function was adopted to fit the LSPR peak (Equation S1)[3]:

$$A = A_0 + \frac{c}{\omega\sqrt{\frac{\pi}{4\ln 2}}} e^{-\frac{4\ln 2}{\omega^2}(\lambda - \lambda_0)^2} \qquad \text{Equation S1}$$

where A, A_0, λ_0, and *w* stand for the absorbance, the baseline, peak position, and the peak width, respectively. The calculation was conducted on OriginPro 2020 (OriginLab, USA).

To quantify the adsorption/desorption processes using Raman spectroscopy, spectral processing, including baseline correction, and data smoothing, was performed on Labspec 6 (Horiba, France).

Simplification of Langmuir kinetics to two-process first-order model

The polynomial expression of the varying-order rate equations for HA adsorption was derived from the work by Liu and coworkers.[4] The adsorption/desorption of HA on particle surface can be considered as a reversible process described below:

$$H + Ag \underset{k_d}{\overset{k_a}{\leftrightarrow}} H - Ag$$ Equation S2

where H is the free HA in the bulk solution, Ag refers to the binding sites on AgNPs surfaces, and H-Ag is the bounded sites by HA molecules on nanoparticle surfaces. k_a and k_d respectively represent the adsorption and desorption rate constants. The fraction (θ_t) of maximum surface coverage by HA at a given time *t* is defined as

$$\theta_t = \frac{q_t}{q_{max}} = \frac{C_0 - C_t}{q_{ma\lambda}X}$$ Equation S3

where q_t and q_{max} are the amounts of HA adsorption by AgNPs at time *t* and the maximum adsorption capacity of AgNPs, respectively. C_0 and C_t are the concentrations of HA in solution at time 0 and *t*, respectively. *X* represents the dosage of AgNPs. According to Langmuir kinetics, the forward adsorption rate is first-order with respect to C_t and (1-θ_t), and the desorption rate is first-order with respect to θ_t.

$$r_a = k_a \mathrm{C}_t \left(1 - \theta_t\right)$$ Equation S4

$$r_d = k_d \theta_t$$ Equation S5

Therefore, the overall adsorption rate can be further expressed as follows:

$$\frac{d\theta_t}{dt} = r = r_a - r_d = k_a \mathrm{C}_t \left(1 - \theta_t\right) - k_d \theta_t$$ Equation S6

Substituting of C_t in Equation S3 into Equation S6 yields

$$\frac{d\theta_t}{dt} = k_a q_{max} X \theta_t^2 - \left(k_a C_0 + k_a q_{max} X + k_d\right)\theta_t + k_a C_0$$ Equation S7

When adsorption reaches equilibrium, $\frac{d\theta_t}{dt}$ equals zero, and θ_t reaches its maximum θ_e. Solving the quadratic function of $\frac{d\theta_t}{dt} = 0$ for the fraction of coverage after equilibrium (θ_e) gives

$$\theta_e = \frac{k_a\left(q_{max}X + C_0\right) + k_d - \sqrt{\Delta}}{2k_a q_{max}X}$$ Equation S8

$$\Delta = k_a^2\left(C_0 - q_{max}X\right)^2 + 2k_a k_d\left(C_0 + q_{max}X\right) + k_d^2$$ Equation S9

After recalculation of Equation S7 and substitution of Equation S8 into Equation S7, $\frac{d\theta_t}{dt}$ can be further simplified

$$\frac{d\theta_t}{dt} = \mathrm{k}_1\left(\theta_e - \theta_t\right)^2 + k_2(\theta_e - \theta_t)$$ Equation S10

$$k_1 = k_a q_{max}X$$ Equation S11

$$k_2 = \sqrt{\Delta}$$ Equation S12

According to Equation S10, the overall adsorption rate, $\frac{d\theta_t}{dt}$, is the combination of the second-order term $k_1\left(\theta_e - \theta_t\right)^2$ and the first-order term $k_2(\theta_e - \theta_t)$. The magnitude of the function depends on the relative value of such two terms, thus leading to the simplification of the overall adsorption kinetics to either the first- or the second-order rate kinetics.

$$k_2\left(\theta_e - \theta_t\right) - k_1\left(\theta_e - \theta_t\right)^2 = \left(\theta_e - \theta_t\right)\left(k_2 - k_1\left(\theta_e - \theta_t\right)\right)$$ Equation S13

If $\left(\theta_e - \theta_t\right)\left(k_2 - k_1\left(\theta_e - \theta_t\right)\right) \gg 0$, then Equation S10 can be simplified as

$$\frac{d\theta_t}{dt} \approx k_2(\theta_e - \theta_t)$$ Equation S14

This is known as the first-order rate equation for adsorption. The sufficient and necessary condition for the Langmuir kinetics to be simplified to the first-order rate equation can be further rearranged to:

$$\theta_t \gg \theta^* = \theta_e - \frac{k_2}{k_1}$$

Equation S15

For the second-order equation of adsorption, $(\theta_e - \theta_t)(k_2 - k_1(\theta_e - \theta_t)) \ll 0$. Equation S13 can be further expressed as:

$$\theta_t \ll \theta^* = \theta_e - \frac{k_2}{k_1}$$

Equation S16

By combining Equation S8, S11, and S12, the following equation can be obtained:

$$\theta_e - \frac{k_2}{k_1} = \frac{k_a(q_{max}X + C_0) + k_d - 3\sqrt{\Delta}}{2k_a q_{max}X}$$

Equation S17

In the adsorption experiments, the dosed HA was far beyond (more than 30 folds) the required amount for monolayer adsorption on nanoparticle surfaces, i.e., $C_0 \gg q_{max}X$ (Figure S5). Therefore, Equation S17 can be further simplified:

$$\theta_e - \frac{k_2}{k_1} \approx - \frac{k_a C_0 + k_d}{2k_a q_{max}X}$$

Equation S18

This is always negative. Then, $\theta_e - \frac{k_2}{k_1} \ll 0 < \theta_t$, which can further deduce that $0 \ll k_2(\theta_e - \theta_t) - k_1(\theta_e - \theta_t)^2$. Therefore, under experimental concentrations, the Langmuir kinetics of ligand adsorption can be simplified to a first-order rate law shown as follows:

$$\frac{d\theta_t}{dt} \approx k_2(\theta_e - \theta_t)$$

Equation S19

Integration of Equation S19 yields:

$$\theta_t = \theta_e - e^{-k_2 t}$$

Equation S20

During the adsorption experiments, θ_t equals to the relative peak shift $(\frac{\Delta\lambda}{\Delta\lambda_e})$ and reach

1 at equilibrium. Therefore, the ligand adsorption in this high ligand concentration regime can be simplified to a first-order kinetic process:

$$\theta_t = \frac{\Delta\lambda}{\Delta\lambda_e} = 1 - e^{-k_2 t}$$

Equation S21

However, due to the complexity of HA, the adsorption dynamics may contain different stages, including the fast and the slow adsorption processes. Therefore, the first-order kinetic process can be further described by a two-process first-order equation:

$$\theta_t = \frac{\Delta\lambda}{\Delta\lambda_e} = \theta_f\left(1 - e^{-k_f t}\right) + \theta_s\left(1 - e^{-k_s t}\right)$$

Equation S22

where subscript *f* & *s* refer to the fast and slow processes, respectively. The relationship between the fraction of maximum surface coverage achieved by the fast (θ_f) or slow (θ_e) process satisfies $\theta_f + \theta_e = 1$. The subscripts *f* & *s* were respectively substituted by 1 and 2 in the manuscript.

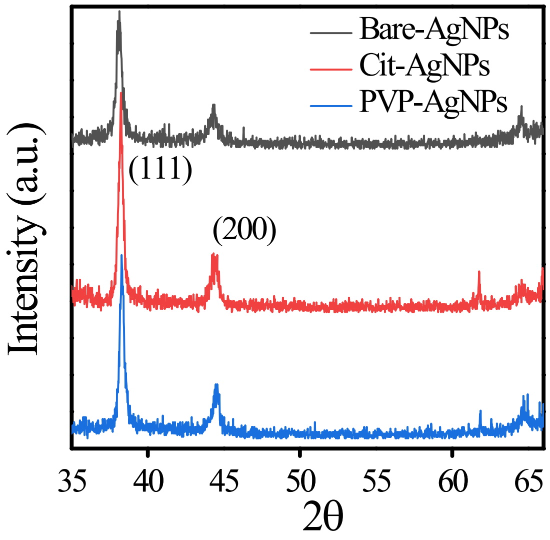

Figure S1. XRD spectra of Bare-, Cit- and PVP-AgNPs.

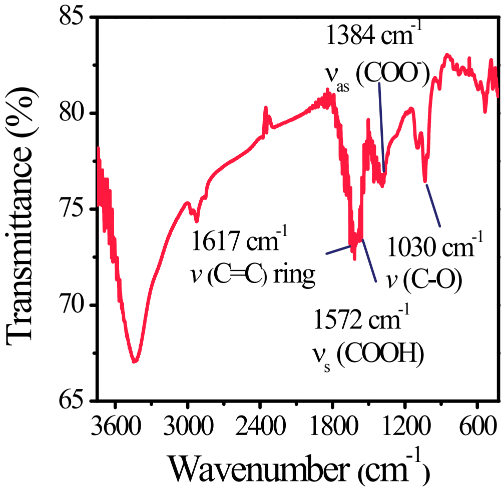

Figure S2. FTIR spectrum of HA and the corresponding peak assignments.

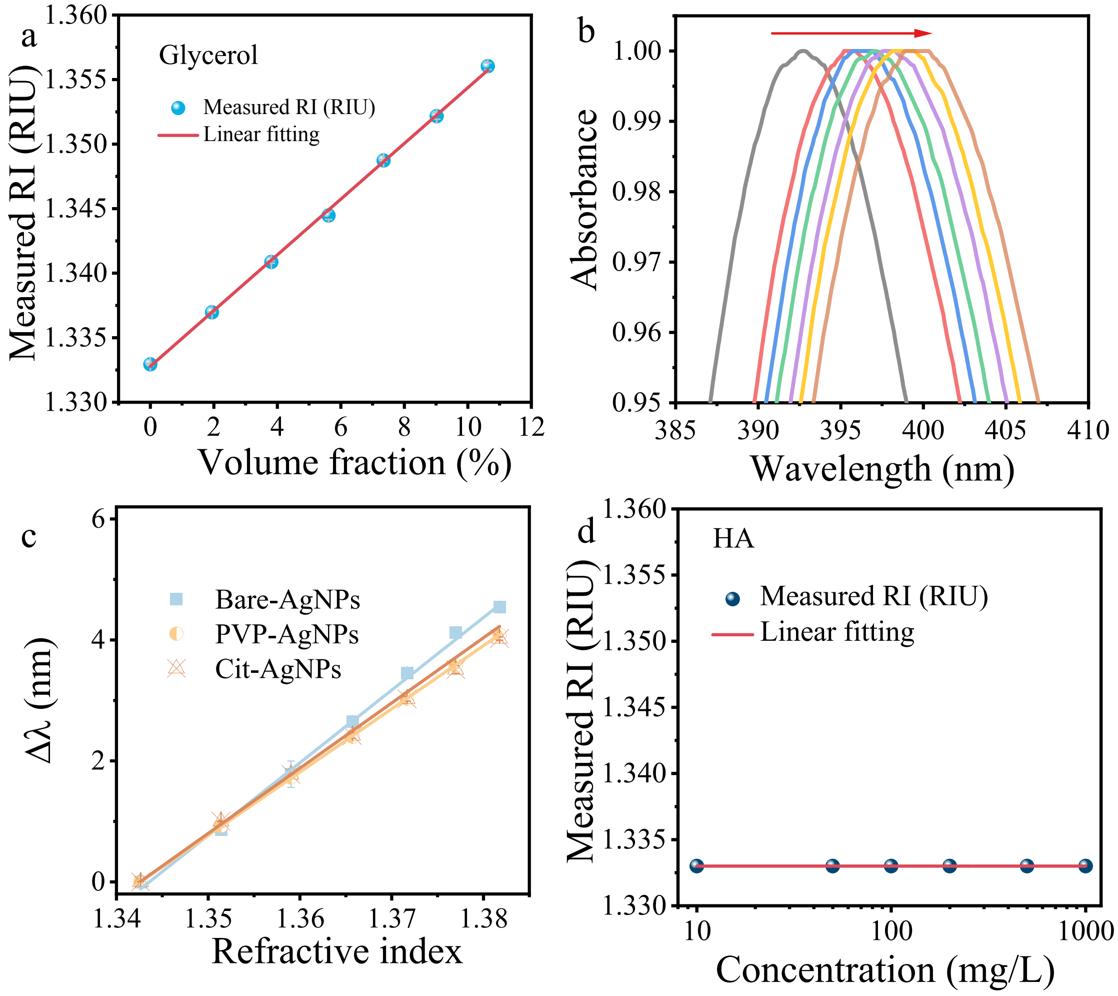

Figure S3. (a) Plot of measured RI of glycerol solution versus its volume fraction. Curve fitting on RI-volume fraction of glycerol shows good linearity (R^2=0.999). (b) Representative red shifts of λ_p after AgNPs being dispersed in different H_2O-glycerol mixtures with increasing glycerol concentrations (from left to right: 0%-38%, volume fraction). (c) Plots of Δλ versus RI for three kinds of AgNPs and the corresponding linearly fitted curves. (d) Plot of measured RI of HA solution versus its mass concentration. The RI of HA solution remained constant with HA concentration ranging from 0 to 1000 mg/L.

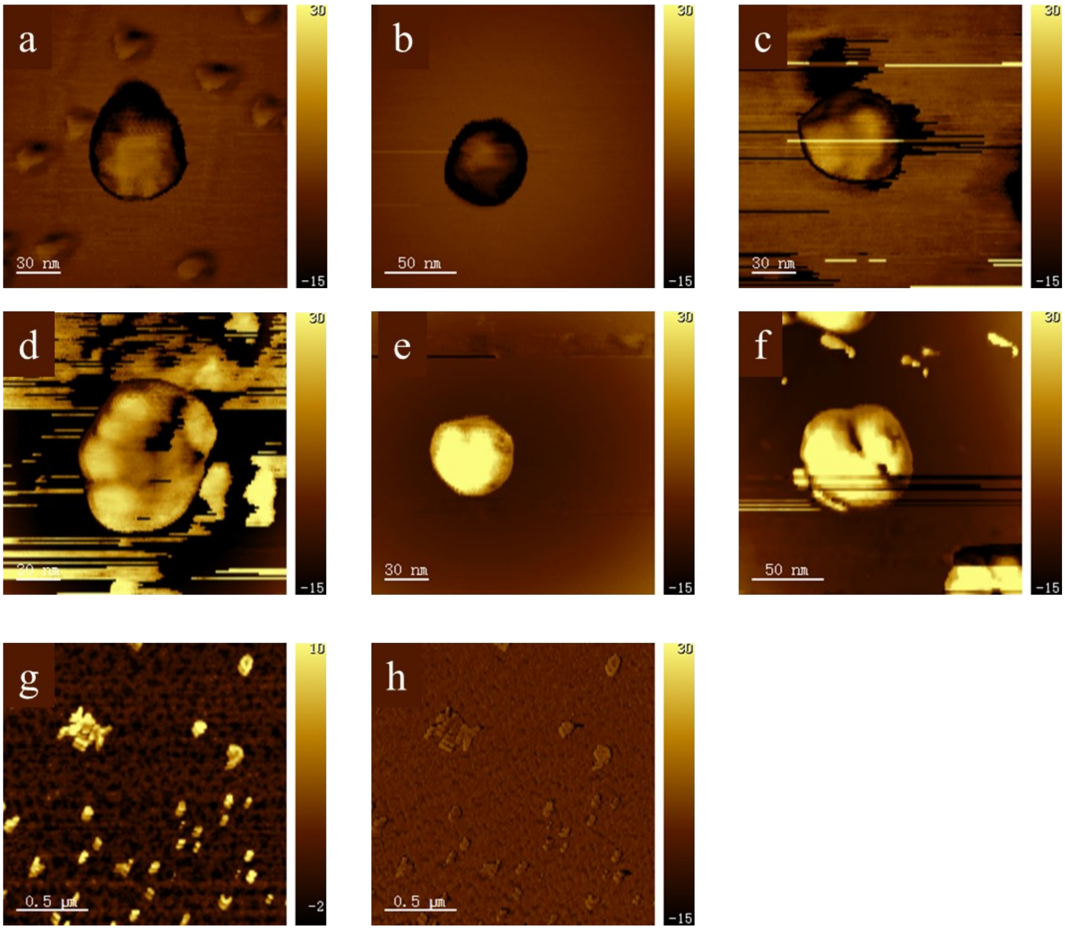

Figure S4. AFM characterization on the formation of HA-corona on AgNPs. Figure a-c denote the AFM phase images of single Bare-, Cit-, and PVP-AgNP, respectively. Figure d-f denote the AFM phase images of single Bare-, Cit-, and PVP-AgNP after their coincubation with HA (125 mg-C/L) for 24 h, respectively. Positive phase shifts were observed after HA-corona formation since the coated HA could alter the tip-nanoparticle surface interactions, including local adhesion, capillary forces, and visco-elasticity. Figure g-h denote the AFM height and phase images of HA on freshly cleaved mica surface. HA shows irregular shapes with positive phase and height of several nanometers.

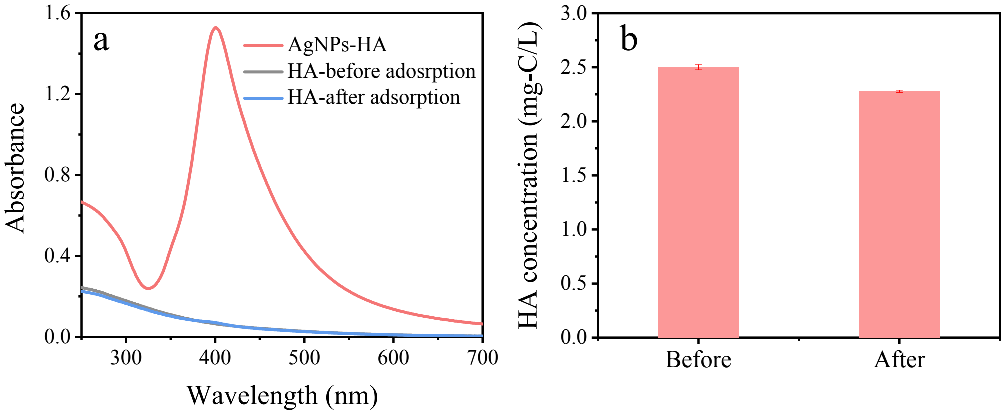

Figure S5. Quantification of HA adsorption on Bare-AgNPs. Bare-AgNPs (13.8 mg-Ag/L) were incubated with HA (2.5 mg-C/L) for 24 h before HA quantification by UV-vis spectroscopy. (a) UV-vis spectra of AgNPs-HA mixture, HA (2.5 mg-C/L) before adsorption, and free HA in the mixture after adsorption. AgNPs were removed from the mixture by centrifugation. (b) Concentrations of free HA molecules before and after incubation. HA concentration was quantified according to the absorbance at 254 nm. The saturated adsorption amount of HA on Bare-AgNPs was calculated as 0.016 mg-C/L HA per mg-Ag/L, which was much less than the dosed HA.

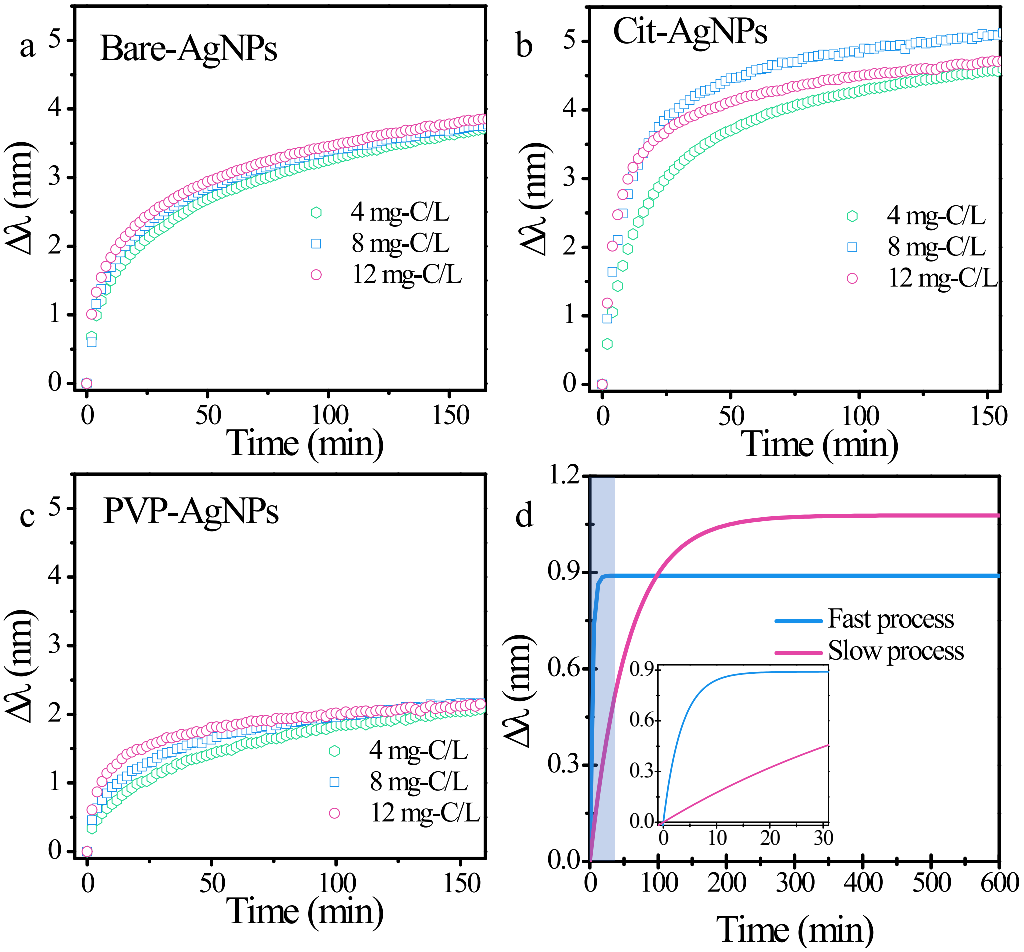

Figure S6. (a-c) Dynamic change of Δλ of Bare-, Cit-, and PVP-AgNPs after dosing 4, 8, and 12 mg-C/L HA. (d) Simulated curves show the coupling of the fast and slow adsorption processes of HA (12 mg-C/L) onto PVP-AgNPs. The inset figure shows the enlarged view of the adsorption kinetics in the initial 30 min.

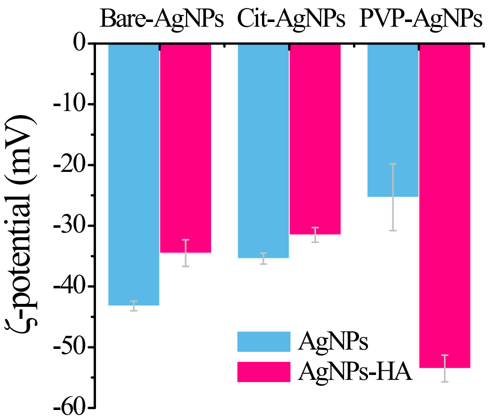

Figure S7. ζ-potentials of AgNPs in the absence or presence of HA (12 mg-C/L).

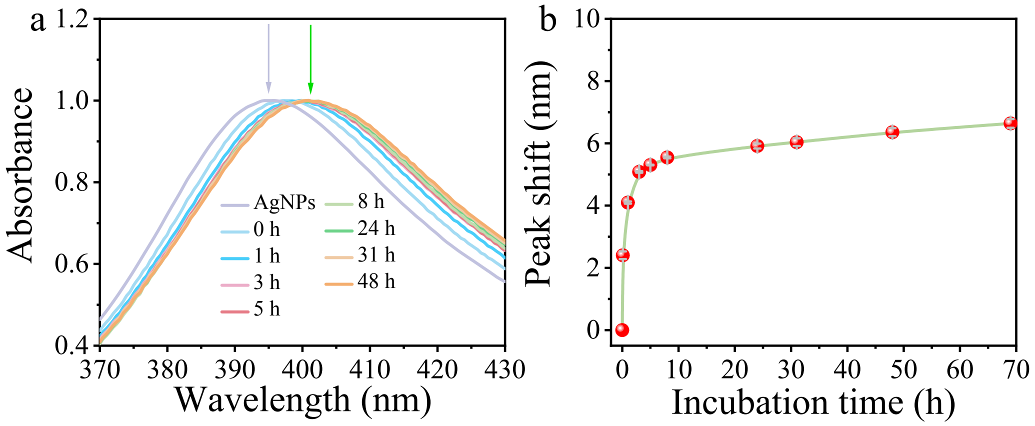

Figure S8. Equilibrium experiment for HA adsorption on AgNPs. (a) Dynamic change of the UV-vis absorbance spectra of Cit-AgNPs (4.6 mg-Ag/L) in the presence of 5 mg-C/L HA. The spectra were normalized according to the maximum absorbance. (b) Dependence of LSPR peak shift on incubation time. All the experiments were conducted in triplicate. HA showed a fast accumulation on Cit-AgNPs in the first 10 h, and reached equilibrium in about 24 h.

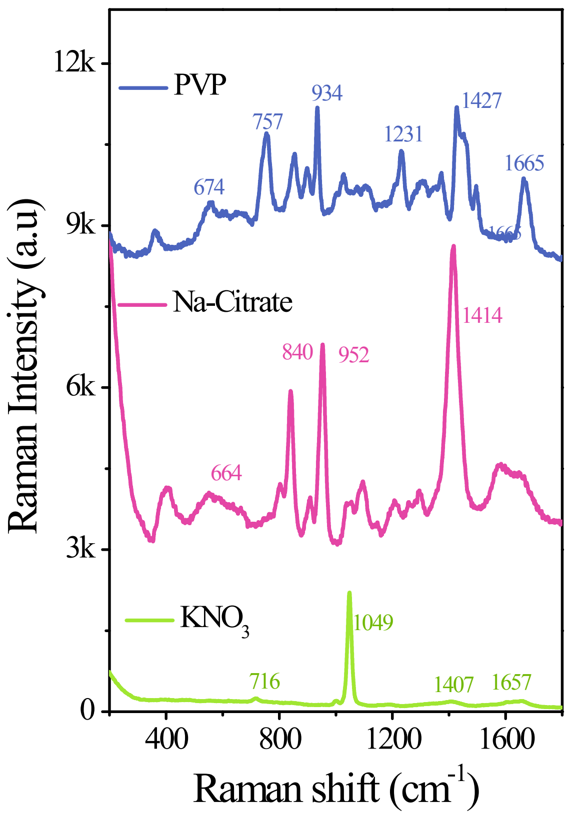

Figure S9. Raman spectra of potassium nitrate (1 M, in H_2O), trisodium citrate (1 M, in H_2O), and PVP (solid).

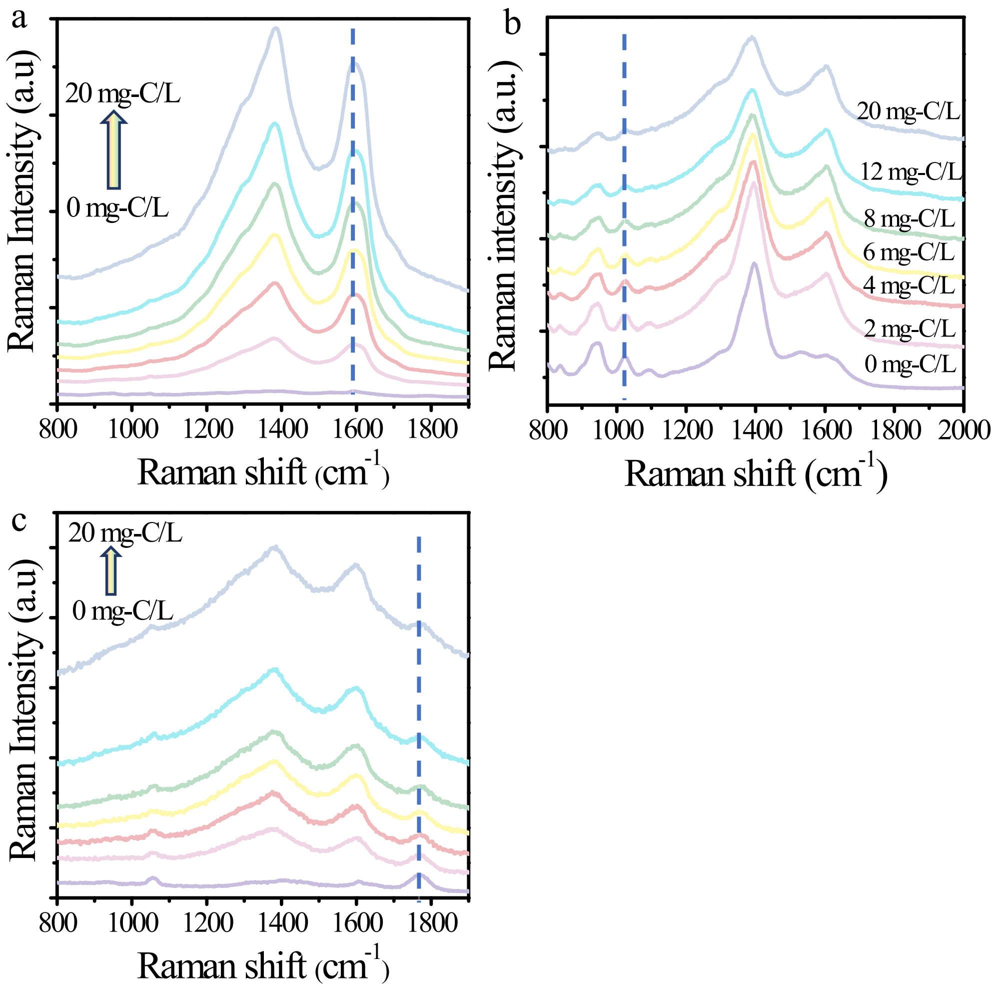

Figure S10. SERS spectra of Bare-AgNPs (a), Cit-AgNPs (b), and PVP-AgNPs (c) in the absence or presence of HA (2, 4, 6, 8, 12, 20 mg-C/L).

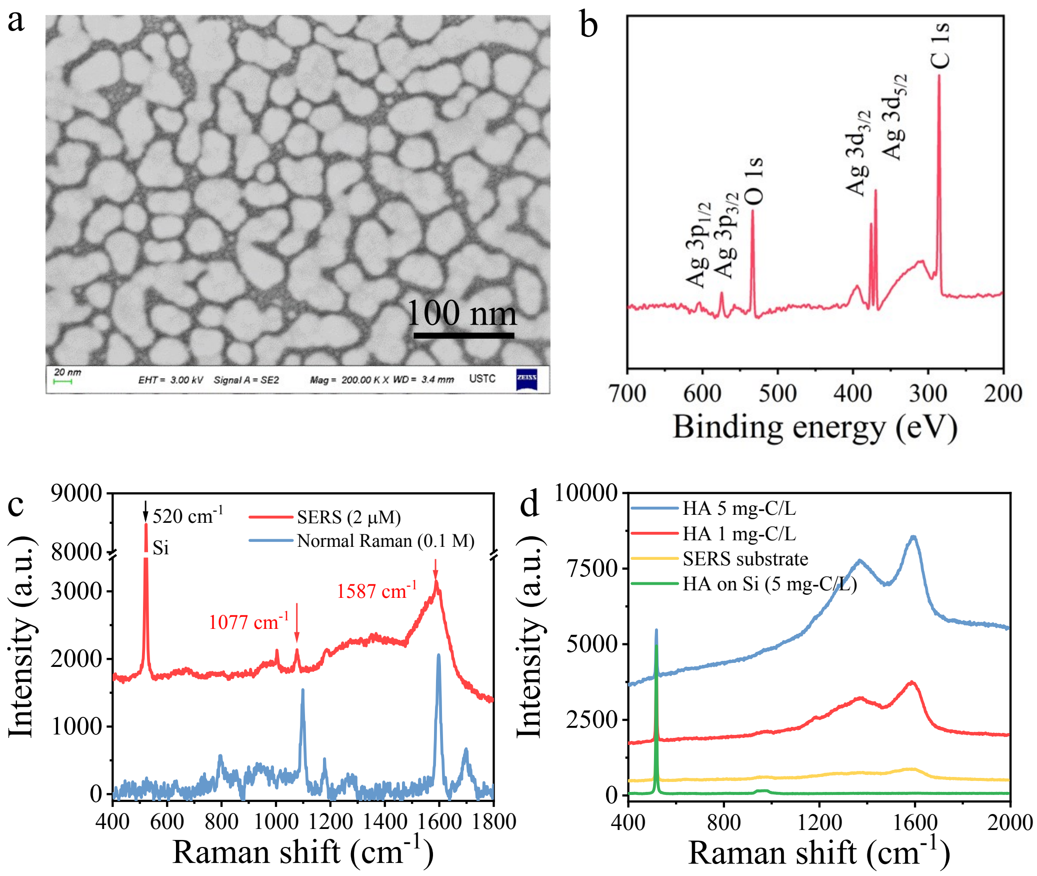

Figure S11. (a) SEM image of AgNPs grown by physical vapor deposition method on silicon substrate; and (b) XPS spectrum of AgNPs on silicon substrate. The SERS performance of AgNPs films was evaluated using 4-mercaptobenzoic acid as the Raman probe. (c) Raman spectrum of 4-mercaptobenzoic acid in ethanol (0.1 M) and SERS spectrum on AgNPs film substrate (2 µM). The arrows indicate the characteristic peaks of Si (520 cm^{-1}) and 4-mercaptobenzoic acid (1077 cm^{-1}, 1587 cm^{-1}). (d) Raman spectra of HA on AgNPs film substrates or on Si wafer. The background spectrum of AgNPs film substrate is also shown. HA on the AgNPs film substrate shows two characteristic peaks, which were not obtained on SERS-inactive substrate (Si wafer), thus demonstrating the ability of AgNPs film substrate toward HA-nanoparticle interaction study.

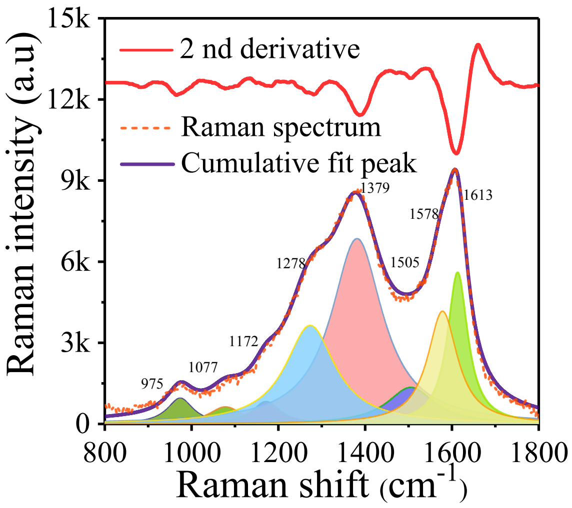

Figure S12. Representative SERS spectrum of HA on Ag substrate. Deconvolution of spectrum (lower panel) was performed into elementary Lorentz components according to the 2nd derivative of the original spectrum (upper panel). The most prominent peaks appeared at 1613, 1578, and 1379 cm^{-1} were assigned to (ν (C=C)), (ν_s (-COOH)), and (ν (-COO$^-$) or ν (C−O) of phenolic -OH), respectively.

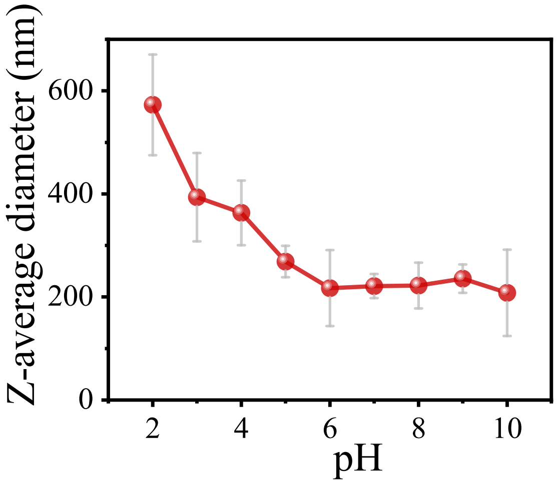

Figure S13. Size change of HA as a function of pH. The hydrodynamic size of HA increased from 221.2 nm at pH 7.0 to 572.8 nm at pH 2.0, implying the inter-molecular aggregation of HA at low pH.

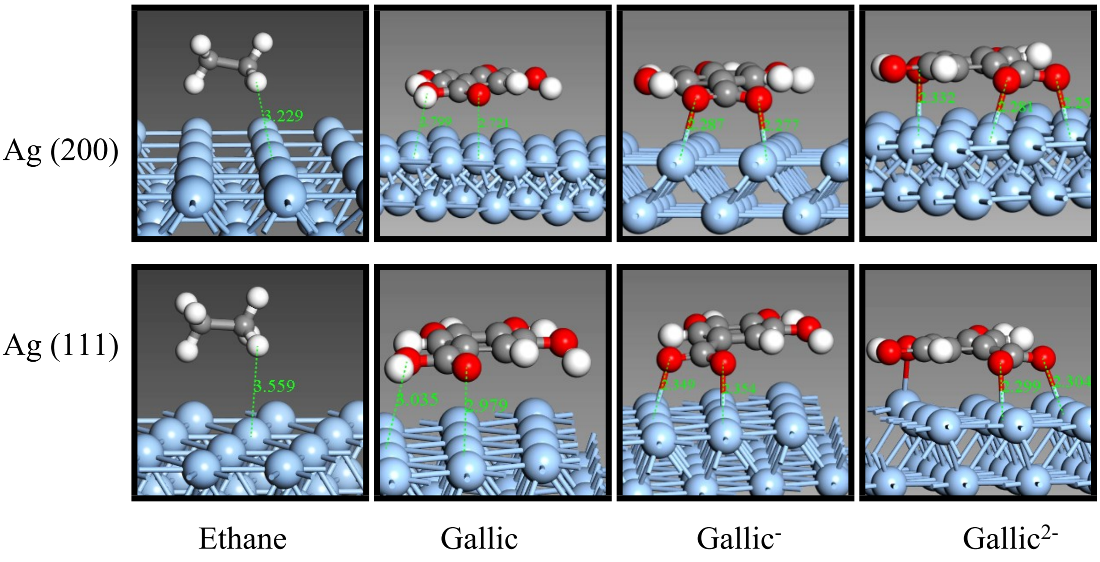

Figure S14. Side view of the binding configurations for adsorbates on Ag (111) and Ag (200). Red, grey, blue, and white atoms stand for O, C, N, and H, respectively. The turquoise-colored crystals below the adsorbates stand for Ag surface. Gallic stands for the fully protonated gallic molecule. Terminal carboxylate group was deprotonated in Gallic$^-$ molecule. Terminal carboxylate and *para*-phenolic -OH were deprotonated in Gallic^{2-} molecule.

Table S1. Elemental analysis of HA

C (%)	H (%)	O (%)	N (%)	S (%)
38.84	3.87	33.11	0.81	0.61

Table S2. Binding energies of deprotonated gallic on different Ag surfaces. The binding configurations of each molecule were shown in Figure S10.

	Ag (111) / eV	Ag (200) / eV
Gallic	0.20	0.37
Gallic^{-}	1.76	2.08
Gallic^{2-}	1.50	2.10

Reference

1. S. Ghosh, H. Mashayekhi, P. Bhowmik and B. Xing, Colloidal stability of Al_2O_3 nanoparticles as affected by coating of structurally different humic acids, *Langmuir*, 2010, **26**, 873-879.
2. Y. Mei, A. Wittemann, G. Sharma, M. Ballauff, T. Koch, H. Gliemann, J. Horbach and T. Schimmel, Engineering the interaction of latex spheres with charged surfaces: AFM investigation of spherical polyelectrolyte brushes on mica, *Macromolecules*, 2003, **36**, 3452-3456.
3. M. Shabaninezhad and G. Ramakrishna, Theoretical investigation of size, shape, and aspect ratio effect on the LSPR sensitivity of hollow-gold nanoshells, *J. Chem. Phys.*, 2019, **150**, 144116-144125.
4. Y. Liu and L. Shen, From Langmuir kinetics to first- and second-order rate equations for adsorption, *Langmuir*, 2008, **24**, 11625-11630.